CdSe Quantum Dot–Fullerene Hybrid Nanocomposite for Solar Energy Conversion: Electron Transfer and Photoelectrochemistry

Jin Ho Bang[†,*] and Prashant V. Kamat[‡,*]

[†]Department of Chemistry and Applied Chemistry, Hanyang University, 55 Hanyangdaehak-ro, Sangnok-gu, Ansan, Kyeonggi-do 426-791, Republic of Korea, and
[‡]Radiation Laboratory and Department of Chemistry and Biochemistry, University of Notre Dame, Notre Dame, Indiana 46566, United States

ABSTRACT

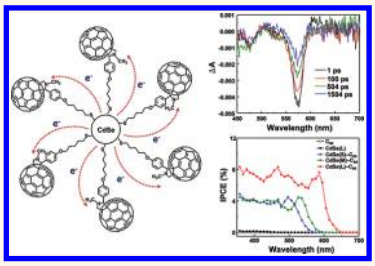

The development of organic/inorganic hybrid nanocomposite systems that enable efficient solar energy conversion has been important for applications in solar cell research. Nanostructured carbon-based systems, in particular C_{60}, offer attractive strategies to collect and transport electrons generated in a light harvesting assembly. We have assembled CdSe–C_{60} nanocomposites by chemically linking CdSe quantum dots (QDs) with thiol-functionalized C_{60}. The photoinduced charge separation and collection of electrons in CdSe QD–C_{60} nanocomposites have been evaluated using transient absorption spectroscopy and photoelectrochemical measurements. The rate constant for electron transfer between excited CdSe QD and C_{60} increased with the decreasing size of the CdSe QD (7.9×10^9 s^{-1} (4.5 nm), 1.7×10^{10} s^{-1} (3.2 nm), and 9.0×10^{10} s^{-1} (2.6 nm)). Slower hole transfer and faster charge recombination and transport events were found to dominate over the forward electron injection process, thus limiting the deliverance of maximum power in CdSe QD–C_{60}-based solar cells. The photoinduced charge separation between CdSe QDs and C_{60} opens up new design strategies for developing light harvesting assemblies.

KEYWORDS: solar cell · quantum dots · fullerene · electron transfer · photoelectrochemistry

Semiconductor nanocrystals (*e.g.*, CdSe, PbS, PbSe, *etc.*) have received great attention in designing next-generation solar cells. Their unique physical properties such as size-dependent electronic structure, large extinction coefficients, and multiple exciton generation render them attractive candidates as photon harvesters.[1−5] A common strategy to effectively harvest solar energy using these semiconductor nanocrystals is to construct nanocomposites having type II band gap alignment. To date, a variety of semiconductor couples have been investigated, and most of the systems are primarily based on inorganic nanocomposites, where large band gap semiconductors, such as TiO_2 and ZnO, are coupled with Cd- or Pb-chalcogenide quantum dots (QDs).[6−15]

In addition to these inorganic nanocomposites, organic/inorganic hybrid nanocomposites have also been found to be useful for the development of solar cells.[16−18] Fullerene-, carbon-nanotube-, and graphene-based nanoheterostructures are representative examples of this sustained effort.[19−27] Especially, fullerene (C_{60}) and its derivatives (*e.g.*, [6,6]-phenyl-C_{61}-butyric acid methyl ester (PCBM)) have long been employed in the construction of polymer-based photovoltaics because of their excellent electron-accepting ability.[28,29] Recently, our group has demonstrated the utilization of C_{60} in QD solar cells by depositing a blend of CdSe QDs and C_{60} on an optically transparent electrode (OTE) using electrophoretic deposition.[30] The photoinduced charge separation achieved in these CdSe–C_{60} assemblies facilitated photocurrent generation in a photoelectrochemical cell. Despite the potential advantage of C_{60} as an electron acceptor, its role in a QD-based light harvesting system has not yet been fully explored. The basic understanding of electron transfer processes of the QD–C_{60} hybrid nanocomposite, therefore, is of particular importance for its effective utilization in solar cells. We have undertaken a systematic study to probe the electron transfer between excited CdSe and C_{60} and to evaluate

* Address correspondence to pkamat@nd.edu, jbang@hanyang.ac.kr.

Received for review May 9, 2011 and accepted November 14, 2011.

Published online November 22, 2011
10.1021/nn204350w

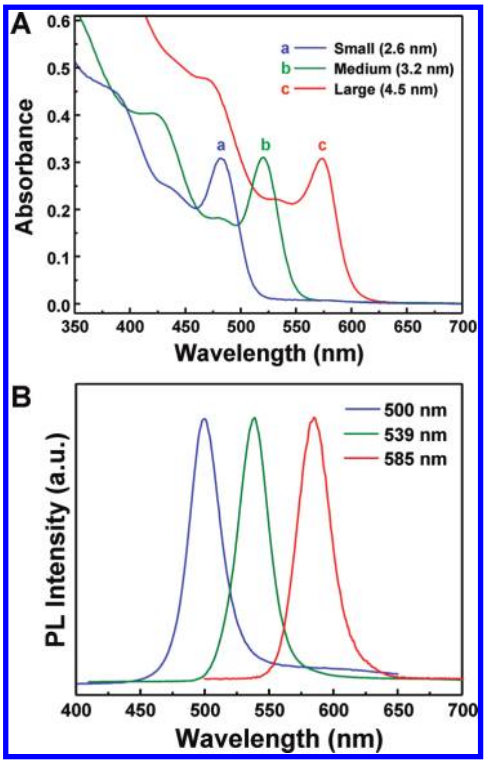

Figure 1. (A) UV–vis absorption spectra and (B) fluorescence spectra of different sized CdSe QDs in toluene.

the photoelectrochemical properties of CdSe QD–C_{60} nanocomposites. In particular, we have focused QD size dependency of the electron transfer properties, and the implication of these results in developing next-generation solar cells is discussed.

RESULTS AND DISCUSSION

Electron Transfer in CdSe QD–C_{60} Nanocomposites. The absorption of CdSe QDs can be tuned by controlling their particle size. In our study, we employed three different sized QDs whose absorption spectra are shown in Figure 1. From the position of sharp, first excitonic peaks, we estimated the particle diameters of CdSe to be 2.6, 3.2, and 4.5 nm,[31] and each QD solution exhibits its characteristic band-edge emission with a small stock shift.

Our earlier work, which focused on using pristine C_{60} to prepare the CdSe–C_{60} composite, produced relatively poor charge separation as realized from the poor photoconversion efficiencies. To circumvent this restraint, we have employed a thiol derivative of C_{60} which enables covalent linking with CdSe QDs. Ability to exchange coordinating ligands with thiol functional groups led us to prepare nanocomposites of CdSe QDs and thiol-functionalized C_{60} (see Figure S1 in Supporting Information for characterization). Such a nanocomposite assembly having CdSe as an electron donor and C_{60} as an electron acceptor functionality facilitates charge separation following band gap excitation of the semiconductor QD (Scheme 1) . Unlike the

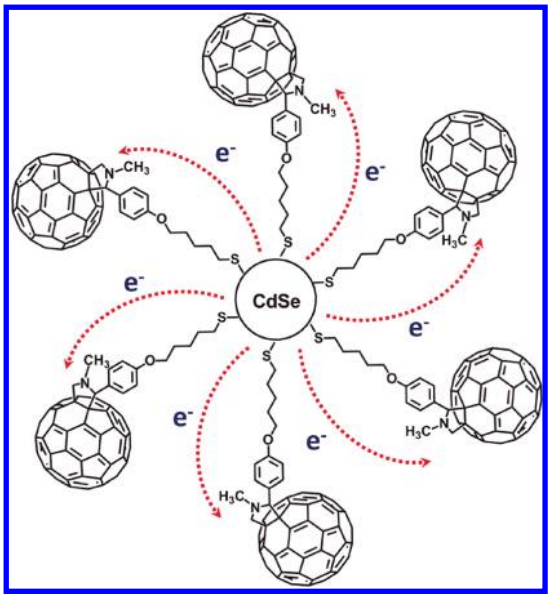

Scheme 1. CdSe QD–C_{60} nanocomposite.

noncovalently linked CdSe QD–C_{60} nanocomposite prepared *via* electrophoretic deposition, these chemically linked CdSe QD–C_{60} cluster assemblies can be readily suspended in nonpolar organic solvents such as toluene, which in turn enabled us to conduct spectroscopic measurements.

Emission quenching of CdSe QDs is a good measure to probe the photoinduced electron transfer process in donor–acceptor assemblies.[10,12] Figure 2 shows the steady-state and time-resolved fluorescence spectra of the largest CdSe QDs, denoted as CdSe (large), suspended in toluene (emission maximum at 585 nm), recorded as thiol-functionalized C_{60} in toluene that was gradually added into CdSe QD solution. With increasing concentration of C_{60}-thiol, we observed a decrease in the emission intensity. Significant emission quenching seen in this experiment confirms the ability of C_{60}-thiol to interact with excited CdSe. In addition, we also monitored the emission lifetime of CdSe QDs at different C_{60}-thiol concentrations. The shorter lifetimes were observed with increasing C_{60}-thiol concentration (Figure S2 in Supporting Information), which further supports faster deactivation of charge-separated states in CdSe QDs *via* electron transfer from CdSe QD to the thiolated C_{60} (reactions 1 and 2).

$$\text{CdSe} + h\nu \rightarrow \text{CdSe(h} + \text{e)} \rightarrow \text{CdSe} + h\nu' \quad (1)$$

$$\text{CdSe–S–C}_{60} + h\nu \rightarrow \text{CdSe(h)–S–C}_{60}^{\bullet -} \quad (2)$$

On the basis of the fluorescence quenching experiment, we estimated that 100–150 thiol-functionalized C_{60} were bound to a single CdSe QD. This estimation is in good accordance with our previous calculation in the case of the gold–C_{60} nanocomposite.[32] Such high local concentration of C_{60} around CdSe QDs is

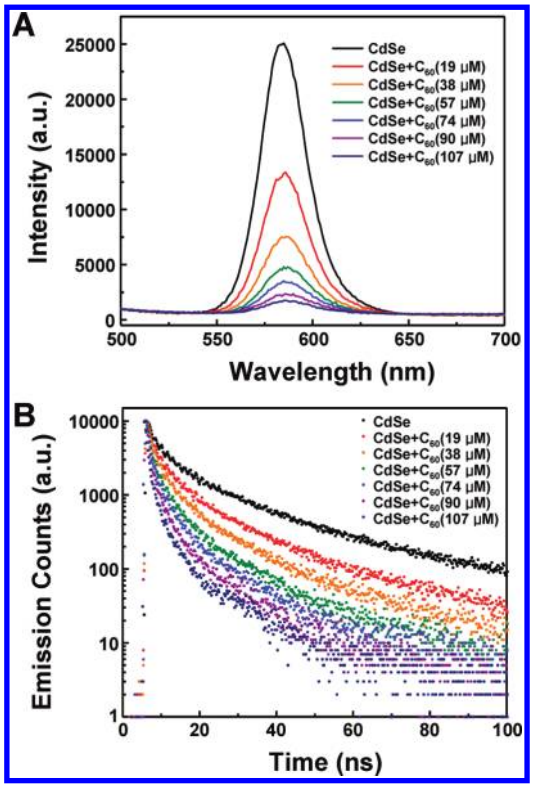

Figure 2. (A) Steady-state fluorescence spectra and (B) time-resolved fluorescence decay spectra of N_2-saturated CdSe QDs (large)−C_{60} nanocomposite solution. Concentration of CdSe QDs in toluene is 0.63 μM.

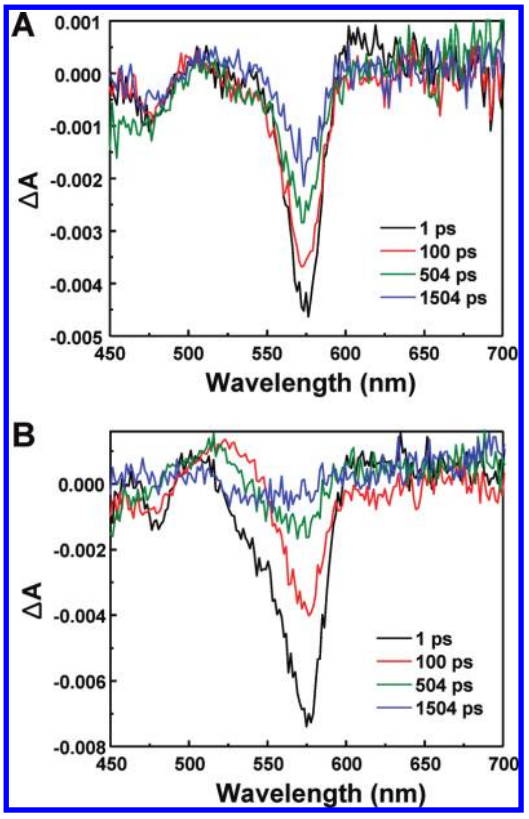

Figure 3. Time-resolved transient absorption spectra recorded following 387 nm laser pulse excitation of (A) CdSe QDs (large) and (B) CdSe QDs (large)−C_{60} nanocomposite solutions in toluene purged with N_2 (0.63 μM CdSe QDs and 90 μM thiolated C_{60} in toluene).

expected to be beneficial for maximizing light harvesting efficiency in our system.

Since the electron transfer in CdSe−C_{60} assembly is likely to occur in subpicosecond to picosecond time frames,[33−38] an ultrafast pump−probe laser spectroscopy was employed to probe the photoinduced charge transfer processes. Figure 3 compares the time-resolved transient absorption spectra recorded following 387 nm laser pulse excitation of CdSe (large) QDs in the absence and presence of thiol-functionalized C_{60}. (Note that the absorption feature of CdSe QDs before and after the addition of thiolated C_{60} remained unchanged; Figure S3 in Supporting Information.) The charge separation following the band gap excitation of CdSe QDs resulted in the bleaching of excitonic bands with maxima at 475 and 573 nm. These bleaching transitions correspond to p-like ($1P_{3/2}$−$1P_e$) and to s-like ($1S_{3/2}$−$1S_e$) states.[38] The bleaching (ΔA) recovery of CdSe QDs (Figure 3A) represents the recombination of photogenerated electrons and holes. When coupled with C_{60}, CdSe QDs encounter an additional deactivation pathway for the photogenerated electrons, thus accelerating the bleaching recovery (presented as decay of ΔA in Figure 3B). This faster bleaching recovery results from electron injection from the conduction band of CdSe ($E_{CB,large}$ = −4.01 eV relative to vacuum) to the lowest-unoccupied molecular orbital (LUMO) of

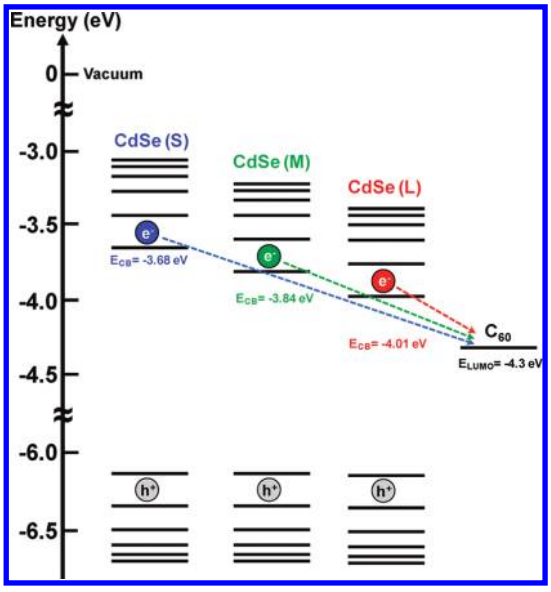

Figure 4. Energy diagram of CdSe QDs used in this study and of C_{60}. The conduction and valence band levels of CdSe QDs are estimated on the basis of our previous studies (ref 40).

C_{60} (E^0_{LUMO} = −4.3 eV relative to vacuum) as the band energy offset favors electron transfer (Figure 4).

The bleaching monitored at each first exitonic peak position (*i.e.*, 482 nm for CdSe (small) and 573 nm for

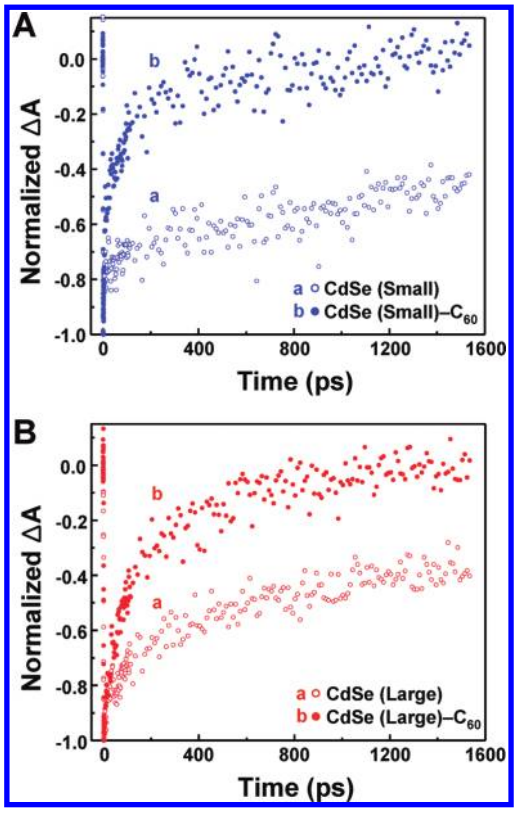

Figure 5. Bleaching recovery profiles of (A) CdSe QDs (small) and CdSe QDs (small)−C_{60} nanocomposite at 482 nm and (B) CdSe QDs (large) and CdSe QDs (large)−C_{60} nanocomposite at 573 nm recorded following 387 nm laser pulse excitation.

CdSe (large)) exhibits faster recovery when CdSe QDs were coupled with C_{60}-thiol regardless of their particle size (Figure 5). As compared in Figure 5, however, the rate of bleaching recovery was dependent on the particle size of CdSe QDs, implying that there is a size dependency on the electron transfer kinetics. Electron transfer kinetics has been described on the basis of the Marcus theory, where free energy driving force (viz., energy difference between donor and acceptor) dictates electron transfer rate.[37,39,40] As the energy difference increases, the rate of electron transfer increases until it reaches a maximum when the driving force is equal to reorganizational energy. Because of band gap tunability in QDs *via* size quantization, the conduction band position of CdSe can be easily modulated. For instance, the conduction band edge of small-sized particles is positioned at less negative energy level than that of larger particles (Figure 4). Given the Marcus model, one could therefore expect faster electron transfer in small-sized CdSe QDs than in larger counterparts when they are coupled with C_{60}.

Since the bleaching recovery profile with time is associated with recombination and electron transfer to C_{60}-thiol, it could be used to elucidate the kinetics of the charge injection process. The recovery of transient bleaching of all CdSe QDs examined in this study was analyzed using biexponential fits (eq 3), and fitted values are tabulated in Table S1 in Supporting Information.

$$y = y_0 + A_1 e^{-t/\tau 1} + A_2 e^{-t/\tau 2} \quad (3)$$

The fitting yields short (τ_1) lifetimes in tens of picosecond time scales and long (τ_2) lifetimes in hundreds of picosecond time scales. These lifetimes are of the same order as that observed in other donor−acceptor nanocomposite systems (*e.g.*, CdSe−TiO_2 and CdSe−carbon nanotubes).[22,37,38] Although it is difficult to resolve the contributions arising from surface heterogeneity and interparticle interactions, one could attribute the short lifetimes to electron transfer from excited CdSe QDs to C_{60}-thiol. The longer lifetimes arise from the electron−hole recombination and back electron transfer from C_{60} to QDs.[38,40] If we assume that the observed fast bleaching recovery component of CdSe−C_{60} system arises solely from the electron transfer, the apparent rate constants of electron injection could be estimated using eq 4:

$$k_{et} = 1/\langle\tau\rangle - 1/\langle\tau_0\rangle \quad (4)$$

where $\langle\tau\rangle$ and $\langle\tau_0\rangle$ are the short lifetimes of CdSe QD−C_{60} and of CdSe QDs, respectively. Using the lifetimes in Table S1, we determined the apparent electron injection rate from CdSe QDs to C_{60} to be 7.9×10^9 (large), 1.7×10^{10} (medium), and 9.0×10^{10} s^{-1} (small). This result indicates that the electron transfer from CdSe to C_{60} indeed occurs on an ultrafast time scale[41] and is consistent with our discussion about the dependency of electron transfer rate on QD size, confirming the energy gap dependence of the Marcus electron transfer theory.

We also obtained a spectroscopic evidence for the electron transfer from the formation of C_{60} radical anion (reaction 2). The electron injection to C_{60} generates the radical anion of C_{60} ($C_{60}^{\bullet -}$), which can be monitored from transient absorption in 1000−2000 nm region. Functional groups of C_{60} have been known to influence the absorption band of the C_{60} radical anion.[25,42] The transient absorption spectra presented in Figure S4 in Supporting Information revealed the characteristic fingerprint of $C_{60}^{\bullet -}$ absorption in the infrared region. Furthermore, the formation of this relatively long-lived transient confirms the electron transfer from excited CdSe QDs to C_{60}. Another interesting aspect is the decay of C_{60} radial anion which exhibits more than 50% decay in 1.6 ns. This observation further points out relatively fast back electron transfer (of the order of 10^8−10^9 s^{-1}) between photogenerated holes in CdSe and C_{60} radial anion.

Photoelectrochemical Properties of CdSe QD−C_{60} Nanocomposites. To investigate photoelectrochemical properties of the CdSe QD−C_{60} couple, the CdSe QD−C_{60} nanocomposites were deposited on OTE and SnO_2-coated OTE by electrophoretic deposition technique.

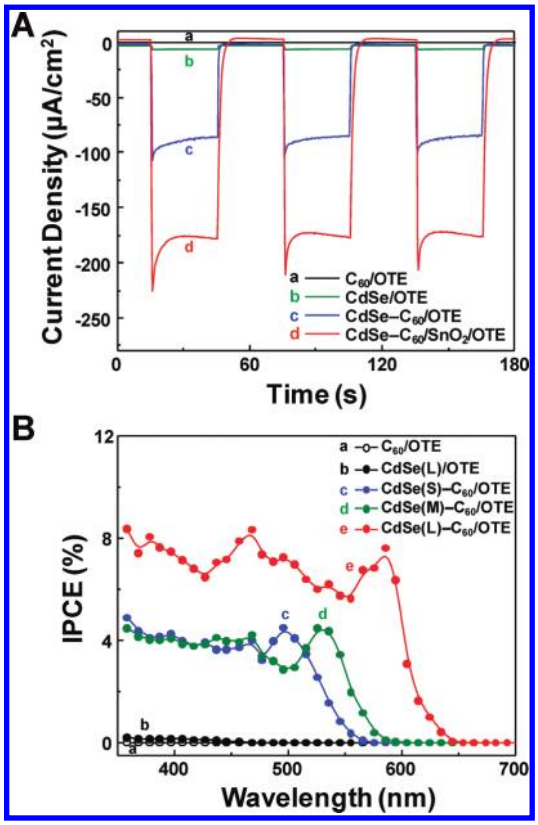

Figure 6. (A) Photocurrent responses of CdSe (large) and CdSe (large)−C_{60} photoelectrodes under white light (λ > 300 nm, 100 mW/cm^2) in 0.1 M Na_2S electrolyte and (B) IPCEs of CdSe QDs and CdSe QD−C_{60} photoelectrodes having different particle sizes of QDs.

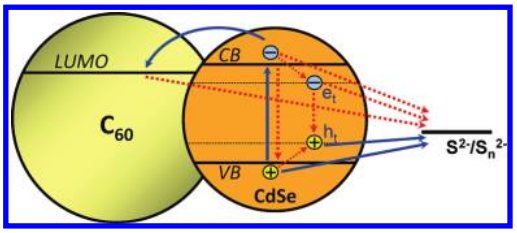

Scheme 2. Charge transfer processes in CdSe QD−C_{60} nanocomposite. Solid, blue lines represent charge transfer processes required for photocurrent generation, whereas dotted, red lines depict main recombination paths to deteriorate the cell performance.

Diffuse reflectance UV−vis spectra (Figure S5 in Supporting Information, part A) show that the prepared photoelectrodes exhibited broad absorption over the visible light region, which is a characteristic optical response of CdSe QDs. Unlike a photoelectrode with CdSe alone, additional absorption features were noticed in the case of the nanocomposite photoelectrode due to the scattering effect of CdSe QD−C_{60} nanocomposite cluster. SEM micrographs display the formation of CdSe QD−C_{60} nanocomposite consisting of 50−100 nm diameter clusters (Figure S5 in Supporting Information, parts B and C) .

Figure 6A compares the photoresponses of four photoelectrodes prepared by electrophoretic deposition. Upon light illumination, prompt photocurrent generation in each electrode was observed, and the photocurrent responses to repeated on−off cycles of light illumination show the stability and reproducibility of photocurrent generation. Bare C_{60} and CdSe QD electrodes produce significantly lower currents than the photoelectrode constructed with CdSe QD−C_{60} nanocomposite, indicating that the dramatically increased photocurrent in the nanocomposite electrode stems from effective charge carrier separation within the nanocomposite *via* electron transfer. Upon inserting a thin SnO_2 layer (E_{CB} = −4.5 eV relative to vacuum) between the nanocomposite layer and OTE, we were able to enhance photocurrent almost twice because this creates a cascaded band alignment where electrons accumulated in C_{60} are further injected into the conduction band of SnO_2, thus facilitating the capture of electrons from $C_{60}^{\bullet-}$.

The incident photon-to-electron conversion efficiency (IPCE) spectra shown in Figure 6B reflect the same trend observed in the photocurrent measurements; only nanocomposite photoelectrodes produced measurable photocurrents under monochromatic illumination. Each CdSe QD−C_{60} nanocomposite electrode shows a similar response with photocurrent onsets at its absorption onset, implying that CdSe QDs are solely responsible for the photocurrent generation. The maximum IPCE of the CdSe (large)−C_{60} photoelectrode was ~8%, whereas those of CdSe (medium)−C_{60} and CdSe (small)−C_{60} photoelectrodes were ~4%. This indicates that bigger CdSe QDs produce twice higher photocurrent than smaller counterparts under monochromatic illumination. Similar observations have been made earlier by the Grätzel group in their study on the CdSe QD−TiO_2 system[43] and by the Fuke and Sykora groups in their recent report on size-dependent light harvesting efficiency of CdSe QDs.[44]

Given the faster electron transfer rates with smaller sized QDs, one would have expected higher IPCE for these systems. The absence of direct dependency between charge injection rate and IPCE parallels our recent study on the effect of different semiconductor oxides on the performance of the CdSe QD solar cell.[40] It is important to note that the photoconversion efficiency of the QD solar cell is collectively influenced by several charge transfer processes (Scheme 2). While electron injection from excited CdSe into the C_{60} donor species and hole capture by S^{2-}/S_n^{2-} redox couple favor higher photoconversion efficiency, the charge recombination between electrons and holes and the electron scavenging by S^{2-}/S_n^{2-} redox couple at the interface contribute negatively. In a recent study, we have shown that the hole capture at the CdSe interface is 2 orders of magnitude slower than electron injection rate ($k_h \approx 10^8$ s^{-1}).[45] In addition, increased charge recombination rates in smaller QD systems could also

contribute to the decreased IPCE. The results presented here highlight the need to better understand various charge transfer steps following initial photoinduced electron transfer and to overcome bottlenecks associated with the charge recombination at the interface and slower hole transfer process. The CdSe–C_{60} system serves as a model system for elucidating various charge transfer processes in the QD solar cell.

CONCLUSIONS

By employing thiol-functionalized C_{60} and CdSe QDs, we were able to develop covalently linked donor–acceptor light harvesting nanocomposites. The electron transfer between excited CdSe and C_{60} is an ultrafast process occurring in the picosecond–nanosecond time scale. The rate constant for electron transfer was dictated by the energy difference between the conduction band edge of CdSe and LUMO of C_{60}, and followed the trend predicted by the Marcus theory. Despite a relatively slower electron injection rate in larger CdSe QDs, the photoelectrode constructed with large nanoparticles exhibited higher energy conversion efficiency than smaller nanoparticles. This observation highlights the fact that the slower hole transfer and faster recombination of charge carriers have more weight in dictating the overall photoelectrochemical performance than the forward electron injection process in the CdSe QD–C_{60} system. The ability to achieve photoinduced charge transfer between CdSe QDs and C_{60} is an important step in designing light harvesting systems. We believe that such molecular acceptors can provide further flexibility in developing next-generation solar cells.

EXPERIMENTAL SECTION

CdSe QDs were prepared by the hot injection method with some modifications.[46] In brief, CdO, tetradecylphosphonic acid (TDPA), trioctylphosphine oxide (TOPO), and dodecylamine (DDA) were degassed at 110 °C and then heated under N_2 to completely dissolve the precursors. Selenium dissolved in trioctylphosphine (TOP) was injected into the hot precursor solution at 315 °C, and subsequent growth was carried out at 270 °C. Upon reaching desired particle size, the solution was cooled to room temperature, washed with a mixture of methanol and toluene, and dissolved in toluene for use. Thiol-functionalized fullerene was synthesized as reported previously[32] and was characterized by a UV–vis spectrophotometer, ^{1}H NMR Varian Inova 500 (500 MHz) spectrometer, and Bruker MicroTOF-II mass spectrometer. For characterization of the CdSe QD–C_{60} nanocomposite, UV–vis absorption, diffuse reflectance UV–vis absorption, and transmission spectra were recorded using a Varian CARY50 Bio UV–vis spectrophotometer and a Shimadzu UV-3101 PC spectrophotometer. Fluorescence spectra were taken using a Horiba Jobin Yvon FluoroMax-3 spectrofluorometer, and fluorescence emission lifetime measurements were carried out using a Horiba Jobin Yvon single photon counting system with a diode laser (373 nm, 250 kHz repetition, 1.1 ns pulse width) as an excitation source. Ultrafast transient absorption spectroscopy was carried out using a Clark-MXR 2010 Ti:sapphire laser system (775 nm, 1 mJ pulse^{-1}, full width at half-maximum of 130 fs, and 1 kHz repetition rate) equipped with a CCD spectrograph (Ocean Optics, S2000-U-UV–vis). Five percent of the fundamental was used to generate a probe pulse, while 95% of the laser beam was utilized by a second harmonic generator to produce a laser pulse for pump (387 nm). Solutions of CdSe QD and CdSe QD–C_{60} in toluene were purged with N_2 prior to the measurement to prevent possible degradation of CdSe QDs during the laser excitation. Transient absorption spectra were recorded at low intensity excitation to prevent Auger recombination of charge carriers. For the preparation of photoelectrodes, CdSe QDs and CdSe QD–C_{60} nanocomposites were electrophoretically deposited onto OTE and SnO_2-coated OTE as previously described in our report,[30] and the morphology of photoelectrodes was examined using a Magellan 400 scanning electron microscope. Photocurrent measurements of CdSe QDs and CdSe QD–C_{60} nanocomposite electrodes were performed using a two-armed cell with a Pt gauze counter electrode in 0.1 M Na_2S solution. A Keithley 2601 sourcemeter was used to collect data, and collimated light (λ > 300 nm, 100 mW/cm^2) from an Oriel 300 W xenon arc lamp was used as the light source. For IPCE measurement, a Bausch and Lomb high-intensity grating monochromator was introduced into the light path to select an excitation wavelength. IPCE was calculated using this equation, IPCE (%) = [1240/λ(nm)][(I_{sc}(A/cm^2)/P_i(W/cm^2)] × 100, where P_i is the power of monochromatic light of wavelength λ (nm) incident on the electrode, and I_{sc} is the short-circuit current.

Acknowledgment. We gratefully acknowledge Drs. K.G. Thomas and A. Wojcik for the synthesis of thiol-functionalized C_{60} and assistance in transient absorption spectroscopy, respectively. The research described herein was supported by the Department of Energy, Office of Basic Energy Sciences and by the Human Resources Development of the Korea Institute of Energy Technology Evaluation and Planning (KETEP) grant (No. 20104010100620) funded by the Ministry of Knowledge Economy, Republic of Korea. This is contribution number NDRL-4881 from the Notre Dame Radiation Laboratory.

Supporting Information Available: Characterization of thiol-functionalized C_{60}; emission decay analysis; UV–vis spectra of CdSe and CdSe–C_{60} dispersed in toluene; observation of radical anion of C_{60} *via* transient absorption spectroscopy; diffuse reflectance UV–vis spectrum and SEM micrographs of electrophoretically deposited CdSe QD–C_{60} nanocomposite film; table of fitted kinetic parameters of bleaching recovery. This material is available free of charge *via* the Internet at http://pubs.acs.org.

REFERENCES AND NOTES

1. Kamat, P. V.; Tvrdy, K.; Baker, D. R.; Radich, J. G. Beyond Photovoltaics: Semiconductor Nanoarchitectures for Liquid-Junction Solar Cells. *Chem. Rev.* **2010**, *110*, 6664–6688.
2. Nozik, A. J.; Beard, M. C.; Luther, J. M.; Law, M.; Ellingson, R. J.; Johnson, J. C. Semiconductor Quantum Dots and Quantum Dot Arrays and Applications of Multiple Exciton Generation to Third-Generation Photovoltaic Solar Cells. *Chem. Rev.* **2010**, *110*, 6873–6890.
3. Hodes, G. Comparison of Dye- and Semiconductor-Sensitized Porous Nanocrystalline Liquid Junction Solar Cells. *J. Phys. Chem. C* **2008**, *112*, 17778–17787.
4. Mora-Sero, I. N.; Bisquert, J. Breakthroughs in the Development of Semiconductor-Sensitized Solar Cells. *J. Phys. Chem. Lett.* **2010**, *1*, 3046–3052.
5. Sambur, J. B.; Novet, T.; Parkinson, B. A. Multiple Exciton Collection in a Sensitized Photovoltaic System. *Science* **2010**, *330*, 63–66.
6. Bang, J. H.; Kamat, P. V. Quantum Dot Sensitized Solar Cells. A Tale of Two Semiconductor Nanocrystals: CdSe and CdTe. *ACS Nano* **2009**, *3*, 1467–1476.

7. Lee, H.; Leventis, H. C.; Moon, S.-J.; Chen, P.; Ito, S.; Haque, S. A.; Torres, T.; Nüesch, F.; Geiger, T.; Zakeeruddin, S. M.; *et al.* PbS and CdS Quantum Dot-Sensitized Solid-State Solar Cells: Old Concepts, New Results. *Adv. Funct. Mater.* **2009**, *19*, 2735–2742.
8. Lee, Y.-L.; Lo, Y.-S. Highly Efficient Quantum-Dot-Sensitized Solar Cell Based on Co-Sensitization of CdS/CdSe. *Adv. Funct. Mater.* **2009**, *19*, 604–609.
9. Bang, J. H.; Kamat, P. V. Solar Cells by Design: Photoelectrochemistry of TiO_2 Nanorod Arrays Decorated with CdSe. *Adv. Funct. Mater.* **2010**, *20*, 1970–1976.
10. Kongkanand, A.; Tvrdy, K.; Takechi, K.; Kuno, M.; Kamat, P. V. Quantum Dot Solar Cells. Tuning Photoresponse through Size and Shape Control of CdSe–TiO_2 Architecture. *J. Am. Chem. Soc.* **2008**, *130*, 4007–4015.
11. Itzhaik, Y.; Niitsoo, O.; Page, M.; Hodes, G. Sb_2S_3-Sensitized Nanoporous TiO_2 Solar Cells. *J. Phys. Chem. C* **2009**, *113*, 4254–4256.
12. Hyun, B.-R.; Zhong, Y.-W.; Bartnik, A. C.; Sun, L.; Abruña, H. D.; Wise, F. W.; Goodreau, J. D.; Matthews, J. R.; Leslie, T. M.; Borrelli, N. F. Electron Injection from Colloidal PbS Quantum Dots into Titanium Dioxide Nanoparticles. *ACS Nano* **2008**, *2*, 2206–2212.
13. Luther, J. M.; Gao, J.; Lloyd, M. T.; Semonin, O. E.; Beard, M. C.; Nozik, A. J. Stability Assessment on a 3% Bilayer PbS/ZnO Quantum Dot Heterojunction Solar Cell. *Adv. Mater.* **2010**, *22*, 3704–3707.
14. Vogel, R.; Hoyer, P.; Weller, H. Quantum-Sized PbS, CdS, Ag_2S, Sb_2S_3, and Bi_2S_3 Particles as Sensitizers for Various Nanoporous Wide-Bandgap Semiconductors. *J. Phys. Chem.* **1994**, *98*, 3183–3188.
15. Zhang, J.; Tang, C.; Bang, J. H. CdS/TiO_2-$SrTiO_3$ Heterostructure Nanotube Arrays for Improved Solar Energy Conversion Efficiency. *Electrochem. Commun.* **2010**, *12*, 1124–1128.
16. D'Souza, F.; Sandanayaka, A. S. D.; Ito, O. SWNT-Based Supramolecular Nanoarchitectures with Photosensitizing Donor and Acceptor Molecules. *J. Phys. Chem. Lett.* **2010**, *1*, 2586–2593.
17. Martínez-Ferrero, E.; Albero, J.; Palomares, E. Materials, Nanomorphology, and Interfacial Charge Transfer Reactions in Quantum Dot/Polymer Solar Cell Devices. *J. Phys. Chem. Lett.* **2010**, *1*, 3039–3045.
18. Kamat, P. V. Graphene-Based Nanoassemblies for Energy Conversion. *J. Phys. Chem. Lett.* **2011**, *2*, 242–251.
19. Robel, I.; Bunker, B. A.; Kamat, P. V. Single-Walled Carbon Nanotube–CdS Nanocomposites as Light-Harvesting Assemblies: Photoinduced Charge-Transfer Interactions. *Adv. Mater.* **2005**, *17*, 2458–2463.
20. Guo, C. X.; Yang, H. B.; Sheng, Z. M.; Lu, Z. S.; Song, Q. L.; Li, C. M. Layered Graphene/Quantum Dots for Photovoltaic Devices. *Angew. Chem., Int. Ed.* **2010**, *49*, 3014–3017.
21. Schulz-Drost, C.; Sgobba, V.; Gerhards, C.; Leubner, S.; Krick Calderon, R. M.; Ruland, A.; Guldi, D. M. Innovative Inorganic–Organic Nanohybrid Materials: Coupling Quantum Dots to Carbon Nanotubes. *Angew. Chem., Int. Ed.* **2010**, *49*, 6425–6429.
22. Farrow, B.; Kamat, P. V. CdSe Quantum Dot Sensitized Solar Cells. Shuttling Electrons through Stacked Carbon Nanocups. *J. Am. Chem. Soc.* **2009**, *131*, 11124–11131.
23. Guldi, D. M. R.; G., M. A.; Sgobba, V.; Kotov, N. A.; Bonifazi, D.; Prato, M. CNT-CdTe Versatile Donor–Acceptor Nanohybrids. *J. Am. Chem. Soc.* **2006**, *128*, 2315–2323.
24. Hasobe, T.; Imahori, H.; Kamat, P. V.; Fukuzumi, S. Quaternary Self-Organization of Porphyrin and Fullerene Units by Clusterization with Gold Nanoparticles on SnO_2 Electrodes for Organic Solar Cells. *J. Am. Chem. Soc.* **2003**, *125*, 14962–14963.
25. Guldi, D. M.; Zilbermann, I.; Anderson, G.; Kotov, N. A.; Tagmatarchis, N.; Prato, M. Versatile Organic (Fullerene)–Inorganic (CdTe Nanoparticle) Nanoensembles. *J. Am. Chem. Soc.* **2004**, *126*, 14340–14341.
26. Gocalińska, A.; Saba, M.; Quochi, F.; Marceddu, M.; Szendrei, K.; Gao, J.; Loi, M. A.; Yarema, M.; Seyrkammer, R.; Heiss, W.; *et al.* Size-Dependent Electron Transfer from Colloidal PbS Nanocrystals to Fullerene. *J. Phys. Chem. Lett.* **2010**, *1*, 1149–1154.
27. Hayashi, H.; Lightcap, I. V.; Tsujimoto, M.; Takano, M.; Umeyama, T.; Kamat, P. V.; Imahori, H. Electron Transfer Cascade by Organic/Inorganic Ternary Composites of Porphyrin, Zinc Oxide Nanoparticles, and Reduced Graphene Oxide on a Tin Oxide Electrode That Exhibits Efficient Photocurrent Generation. *J. Am. Chem. Soc.* **2011**, *133*, 7684–7687.
28. Clarke, T. M.; Durrant, J. R. Charge Photogeneration in Organic Solar Cells. *Chem. Rev.* **2010**, *110*, 6736–6767.
29. Pensack, R. D.; Asbury, J. B. Beyond the Adiabatic Limit: Charge Photogeneration in Organic Photovoltaic Materials. *J. Phys. Chem. Lett.* **2010**, *1*, 2255–2263.
30. Brown, P.; Kamat, P. V. Quantum Dot Solar Cells. Electrophoretic Deposition of CdSe-C_{60} Composite Films and Capture of Photogenerated Electrons with nC_{60} Cluster Shell. *J. Am. Chem. Soc.* **2008**, *130*, 8890–8891.
31. Yu, W. W. Q.; L.; Guo, W.; Peng, X. Experimental Determination of the Extinction Coefficient of CdTe, CdSe, and CdS Nanocrystals. *Chem. Mater.* **2003**, *15*, 2854–2860.
32. Sudeep, P. K.; Ipe, B. I.; Thomas, K. G.; George, M. V.; Barazzouk, S.; Hotchandani, S.; Kamat, P. V. Fullerene-Functionalized Gold Nanoparticles. A Self-Assembled Photoactive Antenna-Metal Nanocore Assembly. *Nano Lett.* **2002**, *2*, 29–35.
33. Boulesbaa, A.; Issac, A.; Stockwell, D.; Huang, Z.; Huang, J.; Guo, J.; Lian, T. Ultrafast Charge Separation at CdS Quantum Dot/Rhodamine B Molecule Interface. *J. Am. Chem. Soc.* **2007**, *129*, 15132–15133.
34. Boulesbaa, A.; Huang, Z.; Wu, D.; Lian, T. Competition between Energy and Electron Transfer from CdSe QDs to Adsorbed Rhodamine B. *J. Phys. Chem. C* **2009**, *114*, 962–969.
35. Huang, J.; Huang, Z.; Yang, Y.; Zhu, H.; Lian, T. Multiple Exciton Dissociation in CdSe Quantum Dots by Ultrafast Electron Transfer to Adsorbed Methylene Blue. *J. Am. Chem. Soc.* **2010**, *132*, 4858–4864.
36. Jin, S.; Lian, T. Electron Transfer Dynamics from Single CdSe/ZnS Quantum Dots to TiO_2 Nanoparticles. *Nano Lett.* **2009**, *9*, 2448–2454.
37. Robel, I.; Kuno, M.; Kamat, P. V. Size-Dependent Electron Injection from Excited CdSe Quantum Dots into TiO_2 Nanoparticles. *J. Am. Chem. Soc.* **2007**, *129*, 4136–4137.
38. Robel, I.; Subramanian, V.; Kuno, M.; Kamat, P. V. Quantum Dot Solar Cells. Harvesting Light Energy with CdSe Nanocrystals Molecularly Linked to Mesoscopic TiO_2 Films. *J. Am. Chem. Soc.* **2006**, *128*, 2385–2393.
39. Gao, Y. Q.; Georgievskii, Y.; Marcus, R. A. On the Theory of Electron Transfer Reactions at Semiconductor Electrode/Liquid Interfaces. *J. Chem. Phys.* **2000**, *112*, 3358–3369.
40. Tvrdy, K.; Frantsuzov, P. A.; Kamat, P. V. Photoinduced Electron Transfer from Semiconductor Quantum Dots to Metal Oxide Nanoparticles. *Proc. Natl. Acad. Sci. U.S.A.* **2011**, *108*, 29–34.
41. Song, N.; Zhu, H.; Jin, S.; Zhan, W.; Lian, T. Poisson-Distributed Electron-Transfer Dynamics from Single Quantum Dots to C_{60} Molecules. *ACS Nano* **2010**, *5*, 613–621.
42. Subramanian, V.; Wolf, E. E.; Kamat, P. V. Catalysis with TiO_2/Gold Nanocomposites. Effect of Metal Particle Size on the Fermi Level Equilibration. *J. Am. Chem. Soc.* **2004**, *126*, 4943–4950.
43. Lee, H. J.; Yum, J.-H.; Leventis, H. C.; Zakeeruddin, S. M.; Haque, S. A.; Chen, P.; Seok, S. I.; Grätzel, M.; Nazeeruddin, M. K. CdSe Quantum Dot-Sensitized Solar Cells Exceeding Efficiency 1% at Full-Sun Intensity. *J. Phys. Chem. C* **2008**, *112*, 11600–11608.
44. Fuke, N.; Hoch, L. B.; Koposov, A. Y.; Manner, V. W.; Werder, D. J.; Fukui, A.; Koide, N.; Katayama, H.; Sykora, M. CdSe Quantum-Dot-Sensitized Solar Cell with ~100% Internal Quantum Efficiency. *ACS Nano* **2010**, *4*, 6377–6386.
45. Chakrapani, V.; Baker, D.; Kamat, P. V. Understanding the Role of the Sulfide Redox Couple (S^{2-}/S_n^{2-}) in Quantum Dot-Sensitized Solar Cells. *J. Am. Chem. Soc.* **2011**, *133*, 9607–9615.
46. Peng, Z. A.; Peng, X. Formation of High-quality CdTe, CdSe, and CdS Nanocrystals Using CdO as Precursor. *J. Am. Chem. Soc.* **2001**, *123*, 183–184.